LYMAN CONTINUUM ESCAPE FRACTION FROM LOW-MASS STARBURSTS AT z= 1.3[*]

Anahita Alavi[1], James Colbert[1], Harry I. Teplitz[1], Brian Siana[2], Claudia Scarlata[3], Michael Rutkowski[4], Vihang Mehta[3], Alaina Henry[5], Y. Sophia Dai [6], Francesco Haardt[7], Micaela Bagley[8]

ABSTRACT

We present a new constraint on the Lyman Continuum (LyC) escape fraction at $z \sim 1.3$. We obtain deep, high sensitivity far-UV imaging with the Advanced Camera for Surveys (ACS) Solar Blind Channel (SBC) on the Hubble Space Telescope (HST), targeting 11 star-forming galaxies at $1.2 < z < 1.4$. The galaxies are selected from the 3D-HST survey to have high Hα equivalent width (EW) with EW > 190 Å, low stellar mass (M$_* < 10^{10}$ M$_\odot$) and U-band magnitude of U< 24.2. These criteria identify young, low metallicity star bursting populations similar to the primordial star-forming galaxies believed to have reionized the universe. We do not detect any LyC signal (with S/N > 3) in the individual galaxies or in the stack in the far-UV images. We place 3σ limits on the relative escape fraction of individual galaxies to be $f_{esc,rel} < [0.10 - 0.22]$ and a stacked 3σ limit of $f_{esc,rel} < 0.07$. Comparing to the confirmed LyC emitters from the literature, the galaxies in our sample span similar ranges of various galaxy properties including stellar mass, dust attenuation, and star formation rate (SFR). In particular, we compare the distribution of Hα and [OIII] EWs of confirmed LyC emitters and non-detections including the galaxies in this study. Finally, we discuss if a dichotomy seen in the distribution of Hα EWs can perhaps distinguish the LyC emitters from the non-detections.

Keywords: galaxies: evolution – galaxies: high-redshift – galaxies: starburst – Reionization

1. INTRODUCTION

Reionization is the last major phase transition in the universe, when Lyman Continuum (LyC) photons ionized the Inter-Galactic Medium (IGM). Hundreds of hours of observations with the leading facilities in the world have been devoted to understanding when and how reionization happened. From observations studying the duration of reionization, it is now believed that the reionization era ended by redshift ~ 6. This has been demonstrated by various methods including the Gunn–Peterson effect in the spectra of high-redshift QSOs (e.g., Fan et al. 2006) and the downturn seen in the fraction of Lyα emitters among Lyman break galaxies beyond z=6 (e.g., Stark et al. 2010; Pentericci et al. 2014; Mason et al. 2019). In addition, the Planck Collaboration et al. (2016) estimate an average redshift between 7.8 and 8.8 for this epoch, adopting an instantaneous reionization model.

However, despite a considerable number of studies, it remains uncertain which sources dominated the emission of LyC photons during the reionization epoch. Both active galactic nuclei (AGN) and young massive stars produce LyC photons and can contribute to the reionization of the IGM. Though, there are some studies indicating that AGNs might be important (Giallongo et al. 2015, 2019), many studies have concluded that they can not be the primary contributors to reionization (e.g., Willott et al. 2005; Siana et al. 2008; Masters et al. 2012; Matsuoka et al. 2018; Parsa et al. 2018; Kulkarni et al. 2019).

In the absence of AGNs, the young massive stars in star-forming galaxies seem to be the primary sources of LyC photons in the early universe. Recent studies (e.g., Bouwens et al. 2017; Livermore et al. 2017; Atek et al. 2018; Ishigaki et al. 2018; Ono et al. 2018; Pelló et al. 2018; Yue et al. 2018) of UV luminosity functions at $z > 6$ have found steep faint-end slopes suggesting a large number density of faint star-forming galaxies at these redshifts. These findings suggest that faint star-forming galaxies may play a significant role during the reionization era (e.g., Robertson et al. 2013; Bouwens et al. 2015; Mason et al. 2015; Robertson et al. 2015). In particuler, (1) faint galaxies must produce sufficient LyC photons and (2) these photons must escape absorption within interstellar medium (ISM) and reach the IGM. The former point can be expected as the faint star-forming galaxies are the most abundant galaxies particularly in the early universe. However, the ionizing photon production rate of these faint galaxies still requires investigation (Emami et al. 2020). To quantify the latter point, we need to measure the fraction of LyC photons that escape (i.e., f_{esc}) the ISM and reach IGM.

A direct measure of f_{esc} at $z > 4$ is difficult due to the high opacity of IGM (Inoue et al. 2014). Therefore, direct study of escaping LyC photons is limited to low and intermediate redshifts. Early studies of the LyC emis-

[1] IPAC, California Institute of Technology, 1200 E. California Boulevard, Pasadena, CA 91125, USA, anahita@ipac.caltech.edu
[2] Department of Physics and Astronomy, University of California, Riverside, CA 92521, USA
[3] Minnesota Institute for Astrophysics, University of Minnesota, Minneapolis, MN 55455, USA
[4] Department of Physics and Astronomy, Minnesota State University, Mankato, MN 56001, USA
[5] Space Telescope Science Institute, 3700 San Martin Drive, Baltimore, MD, 21218, USA
[6] Chinese Academy of Sciences South America Center for Astronomy (CASSACA)/National Astronoical Observatories of China (NAOC), 20A Datun Road, Beijing 100012, China
[7] DiSAT, Universiá degli Studi dell'Insubria, 22100 Como, Italy
[8] Department of Astronomy, The University of Texas at Austin, Austin, TX 78712, USA

sion escaping nearby galaxies (Leitherer et al. 1995; Deharveng et al. 2001; Grimes et al. 2009) resulted only in upper limits, suggesting $f_{\rm esc}$ of a few percent. At higher redshifts ($z \sim 3$), early studies (Shapley et al. 2006; Nestor et al. 2011) reported detections, but several of those detections turned out to be contaminated by foreground sources at lower redshifts (Vanzella et al. 2010, 2012; Siana et al. 2015). Later on, more studies found low redshift contaminants in their sample of LyC emitter candidates (Vanzella et al. 2012; Mostardi et al. 2015; Grazian et al. 2016). Additional high-z studies found null detections and only obtained upper limits (Siana et al. 2007; Iwata et al. 2009; Siana et al. 2010; Boutsia et al. 2011; Rutkowski et al. 2016, 2017; Smith et al. 2018).

Recently, several LyC galaxies have been detected at low ($z < 0.4$; Leitet et al. 2013; Borthakur et al. 2014; Leitherer et al. 2016; Izotov et al. 2016a,b, 2018b,a) and high redshifts (z= 2-4; Shapley et al. 2016; Vanzella et al. 2016; Naidu et al. 2017; Bian et al. 2017; Steidel et al. 2018; Vanzella et al. 2018; Fletcher et al. 2019; Rivera-Thorsen et al. 2019). However, all attempts at intermediate redshifts of $z \sim 1$ have given null results (Malkan et al. 2003; Siana et al. 2007; Cowie et al. 2009; Bridge et al. 2010; Siana et al. 2010; Rutkowski et al. 2016). Although the rate of success in finding LyC emitters at all redshifts has been low, some detections at $z \sim 1$ should have been expected. In fact, there are two reasons that one might expect the detection of LyC emission at $z = 1 - 2$ to be easier than at low redshifts: (1) $z \sim 1$ star-forming galaxies at fixed stellar-masses have higher star formation rates than $z \sim 0$ galaxies (Madau & Dickinson 2014, and references therin) and (2) high-redshift star-forming galaxies have less dust than their low-redshift analogs (e.g., Reddy et al. 2006). The former favors a higher production rate of LyC photons in higher redshift galaxies (see also Matthee et al. 2017). The latter results in less absorption of LyC photons as they travel through the ISM to IGM.

The recent detections of LyC emission have been accomplished with the combination of high sensitivity observations and apparently effective selection techniques. One such technique identifies galaxies with high ratios of [OIII]/[OII], which is potentially associated with density-bounded HII regions. Nakajima & Ouchi (2014) present a photoionization model calculation with CLOUDY (Ferland et al. 1998) that suggests that galaxies with high [OIII]/[OII] ratios are good candidate high $f_{\rm esc}$ objects. They also show that their finding is consistent with the ratio of [OIII]/[OII] $\sim 1 - 4$ of two LyC leakers (Leitet et al. 2011, 2013) known at that time. The potential of this criterion to identify LyC leakers was later investigated in several low-redshift studies of galaxies with [OIII]/[OII] $\gtrsim 5$ (Izotov et al. 2016a,b, 2018b,a), which were successful in finding LyC emitters using the Cosmic Origins Spectrograph (COS) on HST. At high redshift, the first LyC emitter that was discovered, *Ion*2, was found to have a high ratio of [OIII]/[OII] $\gtrsim 10$ (Vanzella et al. 2016). In addition, Faisst (2016) find a positive correlation between the [OIII]/[OII] ratio and $f_{\rm esc}$ compiling thirteen detections and upper limits from the literature. In contrast, Stasińska et al. (2015) argue that this line ratio on its own is not a sufficient diagnostic tool for LyC leakage. This was later validated by several unsuccess-

ful searches of LyC leakage among galaxies with high [OIII]/[OII] ratio (Rutkowski et al. 2017; Naidu et al. 2018) and a statistical analysis by Izotov et al. (2020).

Relatedly, many of the confirmed LyC emitters at high (Vanzella et al. 2016; Naidu et al. 2017; Fletcher et al. 2019) and low redshifts (Izotov et al. 2016a,b, 2018b,a) also display extreme [OIII] EWs. Indeed, extreme [OIII] emitters at $z = 0.1 - 0.3$, known as "Green Pea" galaxies (Cardamone et al. 2009), have long been studied as potential candidates for high LyC escape fraction (Jaskot & Oey 2013; Nakajima & Ouchi 2014; Henry et al. 2015; Izotov et al. 2016a,b, 2018b,a). However, recently, Naidu et al. (2018) found no LyC detection for their sample with high [OIII] EWs, thus raising a question about the reliability of extreme [OIII] EW as an effective tracer of LyC emission. Similar conclusions are also found for individual non-detections at low redshifts by Izotov et al. (2017) and high redshifts by Amorín et al. (2014) and Vasei et al. (2016).

In this paper, we search for LyC photons in low-mass emission line galaxies during a burst in their star formation. We select galaxies to have strong Hα emission lines with rest-frame EW> 190 Å. The Hα line is an indicator of instantaneous SFR, and thus it traces young and hot O-type stars, which are responsible for the LyC production in galaxies. To this end, we conduct a deep far-UV imaging program and exploit the high sensitivity and high spatial resolution of the SBC of the ACS (Ford et al. 1998) onboard HST. Our observations would be sensitive to LyC photons at $z \sim 1.3$, a redshift from which there has been no detections of escaping ionizing radiation to date.

This paper is organized as follows. Section 2 presents the HST observations, reduction of the data and sample selection. In Section 3, we discuss the steps involved in measuring the observed far-UV photometry. In Section 4, we show the results including upper limits to the LyC fluxes of individual galaxies and stacks, and we calculate the upper limit of the escape fraction of ionizing photons. Section 5 compares our study and other LyC efforts in the literature to better understand the galaxy properties that favor LyC leakage.

Throughout the text, we use a flat ΛCDM cosmology with $H_0 = 70$ km s^{-1} Mpc^{-1}, $\Omega_M = 0.3$, and $\Omega_\Lambda = 0.7$. All magnitudes are in the AB system (Oke & Gunn 1983).

2. OBSERVATION AND DATA REDUCTION

2.1. *Sample Selection*

We targeted 11 star-forming galaxies detected by the 3D-HST survey (PI: van Dokkum; Brammer et al. 2012; Momcheva et al. 2016) of the GOODS-South and COSMOS fields with spectroscopic redshifts between $1.2 < z < 1.4$. The lower end of the redshift range is selected to avoid contamination from non-ionizing UV photons redward of the Lyman limit at 912 Å and the upper end ensures high sensitivity to Lyman Continuum photons (see Figure 1).

To select targets from the 3D-HST spectra, we used custom measurements (Rutkowski et al. 2016), made with code originally developed for the WFC3 IR Spectroscopic Parallel survey (WISP; PI:Malkan; Atek et al. 2010). Galaxies are selected to have strong Hα emission

lines with rest-frame EW > 190 Å and stellar masses of $\log(M_*/M_\odot) < 10$. Therefore, our sample includes young, low metallicity, and low-mass star-bursting populations, similar to the class of galaxies believed to reionize the universe. We note that the lower mass selection criterion only excludes two galaxies from our sample as the extreme emision-line selected galaxies (i.e., high EW) have preferentially low stellar continuum and hence low stellar masses. We further require that these galaxies are bright enough that they can provide a meaningful limit to LyC escape fraction, with U-band< 24.2 in the CFHT MegaCam U-band (Erben et al. 2009; Hildebrandt et al. 2009) or the VLT VIMOS U-band (Nonino et al. 2009) images. As a result of this criterion, the selected galaxies have UV luminosities similar to L^*_{UV} at z= 1.3 (using L^*_{UV} estimate from Alavi et al. 2016). Figure 2 summarizes our selection criteria. We plot all of the high Hα EW galaxies within 3D-HST, and show the UV magnitude and stellar mass cut that selects appropriate targets. A list of targets is given in Table 1.

2.2. Observations

The goal of this work is to search for escaping LyC photons from strong emission-line galaxies at $1.2 < z < 1.4$. To this end, we obtained far-UV imaging (program ID 14123, PI: J. Colbert) of our targets using the F150LP filter of SBC on ACS (Ford et al. 1998). This filter has significant transmission in the wavelength range of $1450 < \lambda < 2000$ Å (see Figure 1). The blue cutoff avoids the contamination from the geocoronal emission lines (Lyα and OI lines at 1304 and 1356 Å), which would significantly increase the background in the images. The red cutoff is dictated by the decreasing sensitivity of the Multi-Anode Microchannel Array (MAMA) toward redder wavelengths (Siana et al. 2010). The effective wavelength of this filter is $\lambda_{eff} = 1616.67$ Å, which probes LyC photons at $\lambda_{rest} \sim 700$ Å at $z = 1.3$. We note that most LyC searches including spectroscopic (COS observations of local LyC emitters in Izotov et al. 2016a,b, 2018b,a) and photometric studies (WFC3/UVIS observations of high-redshift LyC emitters in Vanzella et al. 2016; Naidu et al. 2017; Fletcher et al. 2019), are sensitive to LyC flux at 900 Å. The neutral hydrogen opacity at $\lambda_{rest} \sim 900$ Å is about twice of that at $\lambda_{rest} \sim 700$ Å, because the photoionization cross section decreases as ν^{-3}.

The MAMA detector of SBC is a photon-counting device and is not affected by cosmic rays. The detector has no read noise and its primary source of noise is dark current. The SBC dark current has two components. The first is a steady, spatially uniform count rate that does not change with the detector temperature. It is estimated to be a very stable value of 8.11×10^{-6} cts/pix/s (Avila 2017). The second component is a temperature-dependent glow that rises at $T > 25$ °C. In previous studies (Teplitz et al. 2006; Siana et al. 2007; Avila 2017), it has been noted that the variable dark glow is most prominent near the center of the chip and the lower left corner of the detector has a stable dark rate even at elevated temperatures. Therefore, we designed our observations to place all of our targets in the detector corner least affected by the central glow (position $x = 250$, $y = 250$ pixel on the SBC detector), similar to the strategy of
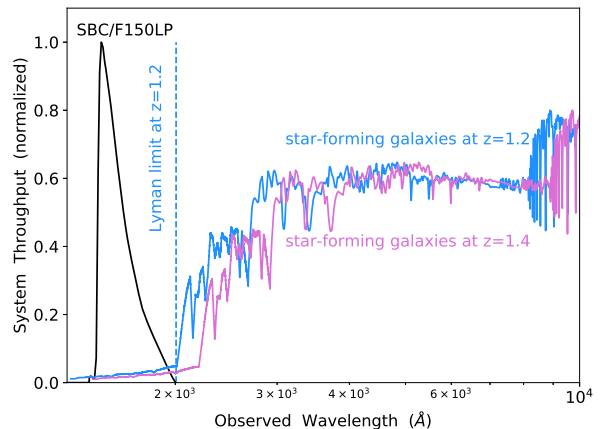

Figure 1. Total system throughput for the ACS SBC/F150LP filter. Two model SEDs of star-forming galaxies at z=1.2 (solid blue) and 1.4 (solid purple), the low and high cuts of our redshift range, are also shown to demonstrate that no non-ionizing flux is entering this system throughput. The SEDs are from BC03 synthetic stellar population models (Bruzual & Charlot 2003) representing of normal star-forming galaxies at $z \sim 1$ with constant SFR, solar metallicity, 100 Myr age and E(B-V)=0.1. The dashed blue line shows the Lyman limit cut at rest-frame 912 Å at $z = 1.2$.
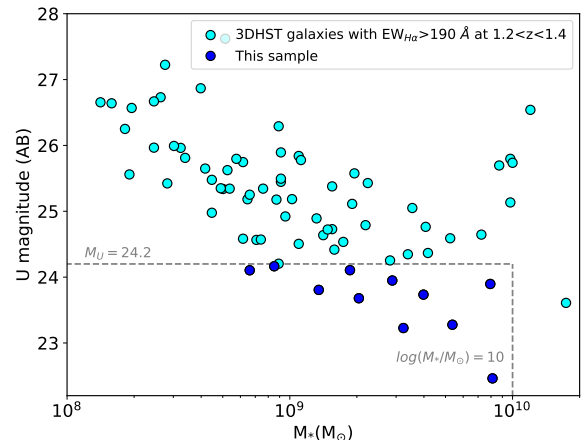

Figure 2. The U-band magnitude versus stellar mass for all of the galaxies with $1.2 < z < 1.4$ and EW(Hα) > 190 Å in the 3D-HST catalogs. The dashed lines show our U-band magnitude and stellar mass cuts at $U = 24.2$ and $\log(M_*/M_\odot) < 10$, respectively. Our final sample consist of 11 sources, which happened to be located in the COSMOS and GOODS-South fields specified as blue circles.

Siana et al. (2010).

Each target is imaged in one visit to a varying depth of one, two or three orbits depending on the galaxy's rest-UV brightness (also see Section 4.3). Each orbit consists of four dithered exposures with similar exposure times of 654s or 692s.

2.3. Data reduction

We downloaded the raw data from the Barbara A. Mikulski Archive for Space Telescopes (MAST), which we then processed using the PYRAF/STSDAS `CALACS` program to subtract the dark current and flat field the images. We use the dark image provided by the STScI as a reference to remove the primary dark component. This

Table 1
SBC Sample

ID	RA [deg]	Dec [deg]	z	EW$_{rest}$($H\alpha$)[Å]	EW$_{rest}$([OIII])[Å]	log(M$_*$/M$_\odot$)[a]	A$_v$[a]	log(SFR)[M$_\odot$ yr^{-1}] [a]
cosmos-1-111	150.07448	2.4172121	1.254	193.0	-*	9.31	0.4	-0.30
cosmos-3-69	150.09259	2.3244885	1.400	201.1	45.6	9.60	0.5	0.61
cosmos-3-113	150.08089	2.3239765	1.257	190.7	160.1	9.27	0.5	0.45
cosmos-7-64	150.06325	2.4488557	1.320	228.8	212.9	9.51	0.1	-0.79
cosmos-13-80	150.12906	2.2307920	1.230	199.1	172.2	9.46	0.6	0.64
cosmos-28-132	150.10593	2.4162436	1.262	498.6	419.7	8.95	0.1	-0.04
goodss-6-124	53.199558	-27.863221	1.231	248.1	485.9	8.82	0.0	0.42
goodss-9-108	53.062504	-27.764822	1.232	193.0	197.7	9.13	0.1	0.31
goodss-21-24	53.198181	-27.878668	1.253	226.6	110.6	9.91	0.3	1.09
goodss-27-124	53.193836	-27.844275	1.237	344.4	738.1	8.93	0.0	0.27
goodss-30-67	53.099816	-27.730301	1.309	260.5	205.4	9.73	0.2	0.83

[a] All physical properties are from our SED fitting.
* The [OIII] line for this source is very noisy and the line-fitting is uncertain. Therefore, we do not use the [OIII] EW estimate for this source.

dark component does not account for the central glow which rises with temperature. This excess dark component is later subtracted as explained in Section 2.4. The `Astrodrizzle` code was then used to combine the exposures and make the final drizzled image. Here, we weight the individual frames by their exposure time and we set the output pixel scale to 0.03″and the pixfrac to 1. Because the SBC data have little sky background and are insensitive to cosmic rays, the sky subtraction and cosmic ray rejection steps have been turned off in running the `Astrodrizzle` code.

The images are drizzled and aligned to the CANDELS F606W tiles. The relative astrometry between SBC and reference images is always better than 1-1.5 pixels (i.e., the rms of the best alignment fit). We note that the popular `Tweakreg` code for the HST image alignment fails due to lack of an adequate number of compact, bright sources. Therefore, we manually identify matching sources on the individual science and reference images, and then use the `PYRAF geomap` code to calculate the shift between the images.

We note that we could only align the images of 7 sources. For the remaining 4 (with IDs cosmos-7-64, cosmos-9-108, goodss-21-24, and goodss-30-67), no sources were detected in the individual SBC/F150LP images to be used for the alignment. Unless otherwise noted, we drop these 4 objects from the LyC analyses presented in this paper. Similar to the sample of 7 sources that we will be discussing, we did not detect any LyC flux for these 4 objects in the F150LP images.

2.4. Dark subtraction

As stated above, dark current is the dominant source of noise in these observations and a careful treatment of dark subtraction and its varying component is vital. Here, the total dark is a sum of the primary and excess dark components. We subtract these dark components separately in two stages.

First, we subtract the primary calibration dark reference file [10], which accounts for the low and stable dark current of 8.11×10^{-6} counts s^{-1} pix^{-1} when the instrument is < 25 °C. As explained in Section 2.3, the primary dark subtraction is part of the image processing

[10] We downloaded the reference file $04k1844aj\_drk$ from the HST Calibration Reference Data System (CRDS).

done by the `CALACS` program.

Second, although each target is located in the least affected region on the detector, we check for additional dark current associated with the central glow. First from a visual inspection of different exposures in the image of each target, we define a border separating the corner with stable background from the central region with varying dark glow. We exclude those regions of the image where there are sources using a segmentation map from a `SExtractor` (Bertin & Arnouts 1996) run on F606W images. Using the F606W photometric aperture of each target (see Section 3), we then generate random apertures within the corner of each image and investigate the distribution of total flux within these regions. If the primary calibration dark image were adequate, we would expect each flux distribution to be centered at zero. However, these flux distributions are centered around non-zero values varying between $[5.0, 11.0] \times 10^{-6}$ counts s^{-1} pix^{-1}. This is evidence of an excess dark current with a value of $\pm 30\%$ of the primary dark current (i.e., excess dark $= (1 \pm 0.3) \times$primary dark). Therefore, for each drizzled image, we subtract the median of the flux distribution of the random apertures within the corner. We use these improved drizzled images for our LyC analyses.

This excess dark current appears to increase with the detector temperature. We also investigate the possibility of a gradient in the excess dark and we find that it rises from corner edge toward the center by about 30%. However, this dark gradient does not affect our photometry because our sources are compact. Overall, these behaviors are consistent with those reported in Teplitz et al. (2006), Siana et al. (2007), and Avila (2017). However, our estimate of the excess dark current in the corner is much weaker than what these studies have reported for the central dark glow, thanks to our mitigation strategy.

3. PHOTOMETRY

For the UV, optical and Near-IR photometry, we use the public 3D-HST catalogs of COSMOS and GOODS-South fields (Brammer et al. 2012; Skelton et al. 2014). They assembled the catalogs using a combination of three Wide Field Camera 3 (WFC3; MacKenty et al. 2010) bands of F125W, F140W and F160W for detection and the PSF-matched HST images of each field. For each galaxy, we use ground-based U-band ($\lambda_{rest} \sim 1600$ Å) from CFHTMegaCam or VLT VIMOS and HST/SBC

F150LP images to compute the observed non-ionizing and ionizing UV (i.e., LyC) fluxes, respectively.

To define apertures for LyC measurements, we started with the SExtractor segmentation maps of the 3D-HST catalogs. However, these photometric apertures are much larger than the area where we expect a significant rest-frame far-UV flux from each galaxy. Therefore, we define new isophotal apertures using shorter wavelength filters, which probe the rest-frame near-UV and thus areas of ongoing star formation in galaxies. Ideally, we would use the U-band images as our detection band but they are low-resolution ground-based data and require degrading the SBC images. We therefore choose to run the SExtractor in dual image mode using the optical F606W image, which corresponds to rest-frame $\lambda \sim 2600$ Å, for detection. We note that this is the same Sextractor measurement that was referred to in Section 2.4. Because the F606W image is deep (i.e, with 5σ depth of 28.3 and 29.4 magnitudes for COSMOS and GOODS-South, respectively), the isophotes are large. Using a solution discussed in Siana et al. (2007), we find that if we shrink the isophotes to include 80% of the F606W total flux, the area decreases by a factor of 1.5-2.7. This increases our far-UV sensitivity by 0.2-0.5 magnitude.

We calculate the 3σ upper limits of the LyC fluxes in two ways:

- As explained above, the dark current is the dominating component of noise in the SBC images. We estimate the total dark current from the sum of the primary dark and excess dark component (see section 2.3) within the isophotal aperture of each target. The total noise is then calculated as $\sqrt{\text{Total Dark} \times \text{Exposure time} \times \text{Area}_{\text{isophot}}}$.

- We first use the F606W isophotal segmentation map to exclude all objects from the SBC images. We then randomly move the isophotal aperture of each target within the image corner where it is located and measure the flux within the aperture. The final noise is then derived from the standard deviation of the distribution of random aperture fluxes.

Our estimates of the limits from these two measurements agree within 10%. Unless otherwise noted, we use the limits from the second technique as listed in Table 2.

Finally, we correct the photometry for Galactic extinction using the values of $A_V = 0.051$ & 0.021 mag for COSMOS and GOODS-South, respectively, as reported in Skelton et al. (2014). These Galactic dust extinction values are based on the recalibration by Schlafly & Finkbeiner (2011) of the COBE/DIRBE and IRAS/ISSA dust maps. Assuming a Cardelli extinction curve (Cardelli et al. 1989) with $R_V = 3.1$, we estimate the $A_{1600} = 0.13$ & 0.05 mag, respectively.

4. RESULTS

4.1. *Individual galaxies*

We do not detect any individual galaxy with $S/N > 3$ in the SBC LyC images. Figure 3 shows the postage stamps of SBC far-UV and F606W images of each of the targets. The distribution of S/N values calculated using the second technique is shown in Figure 4. The distribution of the S/N is centered around zero with a mean value of -0.07 and standard deviation of 0.9. We also search for LyC flux that may exist offset (up to $2''.0$) from the UV continuum as discussed in Iwata et al. (2009) and Nestor et al. (2013).

4.2. *Stack*

We stack the far-UV F150LP cutout images to estimate an average escape fraction. To display the stacked image (see Figure 5), we do a simple addition of F150LP $3'' \times 3''$ cutouts, centered at the position of each source in the F606W image. As shown in Figure 5, we do not detect a signal in the stacked image. We note that because galaxies have various sizes and morphologies, in the case of a simple addition, some galaxies will add noise to areas where other galaxies have flux. Therefore, to measure the stacked flux, we perform an optimized stacking (see Siana et al. 2010) by only summing the pixels that were in the isophotal segmentation of individual galaxy photometry (see Section 3). We also measure the total noise in the stack by adding the noise (i.e., $\sqrt{\text{Dark} * \text{Exposure Time}}$) in quadrature in the pixels of individual galaxies that were used in the optimal stacking. The total LyC flux in the stack image is $0.3 \times 10^{-31} \pm 1.1 \times 10^{-31}$ erg s^{-1} cm^{-2} Hz. The 3σ limit of the stacked flux is reported in table 2.

4.3. *Escape Fraction of Ionizing Photons*

Lyman continuum radiation produced by young and hot stars is absorbed by neutral hydrogen inside galaxies and dust in the ISM, preventing that radiation from escaping the galaxy and reaching the IGM. There are two broadly-used definitions for the LyC escape fraction in the literature.

First, the *absolute escape fraction, $f_{esc,abs}$*, is simply the fraction of intrinsic LyC photons that escape into the IGM. This definition is convenient to use in theoretical and simulation studies where the true number of LyC photons produced is known from the star formation rate and initial mass function. However, this quantity is difficult to measure in observational studies because it requires a measure of the intrinsic production rate of ionizing photons (i.e., LyC luminosity). The intrinsic LyC luminosity is usually estimated from nebular emission lines such as Hα or from the best-fit SED to the galaxy photometry. Both of these techniques need an understanding of the dust attenuation (i.e., dust extinction model) and thus they suffer from the associated uncertainties. For example, Steidel et al. (2018) show that changing the attenuation relation could change the estimated $f_{esc,abs}$ by a factor of more than three.

The second definition, first introduced by Steidel et al. (2001), is the *relative escape fraction, $f_{esc,rel}$*, referring to the fraction of LyC photons that escape the galaxy relative to the fraction of escaping non-ionizing photons at 1500 Å. A benefit of this quantity is that it is independent of uncertainties in the estimation of dust correction. The $f_{esc,rel}$ can be expressed as below:

$$f_{\text{esc,rel}} = \frac{f_{\text{LyC}}^{\text{out}}/L_{\text{LyC}}^{\text{int}}}{f_{1500}^{\text{out}}/L_{1500}^{\text{int}}} = \frac{(f_{\text{LyC}}/f_{1500})^{\text{out}}}{(L_{\text{LyC}}/L_{1500})^{\text{int}}} \qquad (1)$$

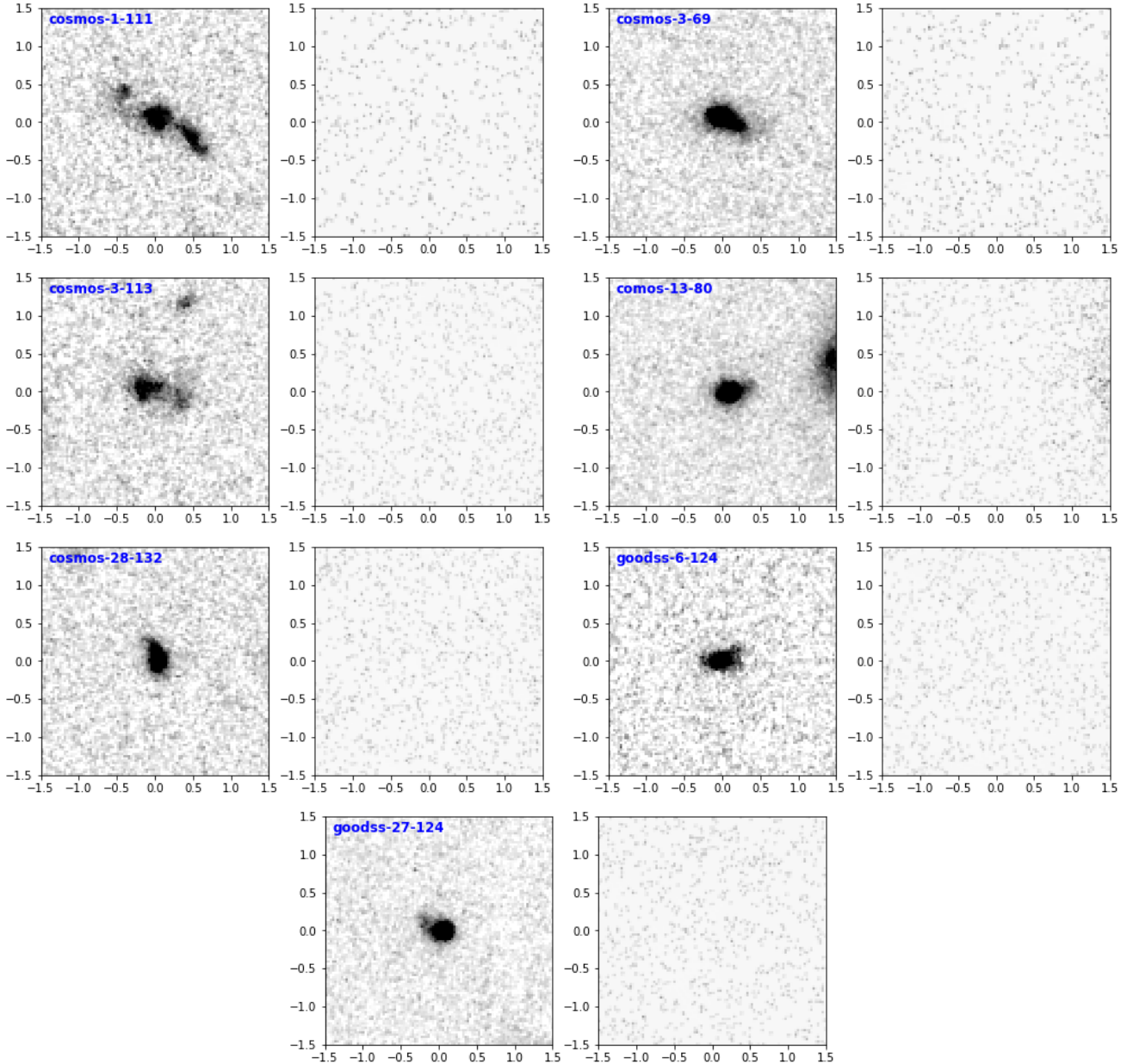where the f_{LyC}^{out} is the LyC flux density per unit fre-

Figure 3. The postage stamps of CANDELS F606W (left) and far-UV F150LP (right) of our targets. Each image is $3''$ on a side. Most of these galaxies (except cosmos-1-111 and cosmos-3-113) display small and compact sizes. As seen in these images, none of these galaxies are detected in the F150LP images.

quency in the vicinity of galaxy right after escaping the ISM. Also, f_{1500}^{out} is the flux density per unit frequency measured at 1500 Å after passing through the galaxy ISM. These flux values are related to the observed fluxes as follows:

$$\left(\frac{f_{\mathrm{LyC}}}{f_{1500}}\right)^{\mathrm{out}} = \left(\frac{f_{\mathrm{LyC}}}{f_{1500}}\right)^{\mathrm{obs}} \times e^{\tau_{\mathrm{IGM}}(\mathrm{LyC})} \qquad (2)$$

where $\tau_{\mathrm{IGM}}(\mathrm{LyC})$ is the optical depth of LyC photons through the IGM along the line of sight to that galaxy. We note that we measure the LyC flux at 700 Å, while it is usually measured at 900 Å in most studies (e.g., Steidel et al. 2001; Izotov et al. 2016a,b; Marchi et al. 2017; Steidel et al. 2018; Fletcher et al. 2019). Considering current observational facilities (i.e, SBC), we only have

access to the ionizing flux at shorter wavelengths (700 Å) at $z \sim 1$ (see also Siana et al. 2007, 2010).

As seen in equations 1 and 2, to derive $f_{esc,rel}$, we need to estimate the IGM absorption and the amplitude of the intrinsic stellar Lyman break, $(L_{1500}/L_{LyC})^{\mathrm{int}}$. Below, we summarize what we use for each of these quantities.

IGM: The IGM absorption $(e^{-\tau_{\mathrm{IGM}}})$ is computed from a Monte Carlo simulation described in detail in Siana et al. (2010) and Alavi et al. (2014). In summary, we create 300 different lines-of-sight through the IGM at different redshifts by selecting random hydrogen absorbing systems (i.e., Lyα forest, Lyman limit and damped Lyα systems) from the density distribution associated with that redshift. We chose to run this simulation for 300
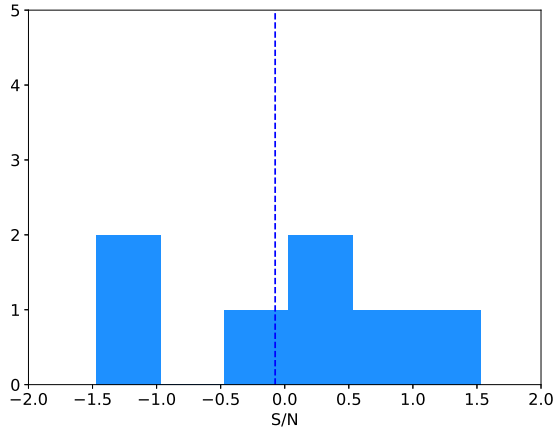
Figure 4. The distribution of measured S/N of LyC fluxes for our sample of 7 galaxies. There is no detection above S/N> 3. The distribution is nearly centered at zero with the dashed line indicating the arithmetic mean value at -0.07.
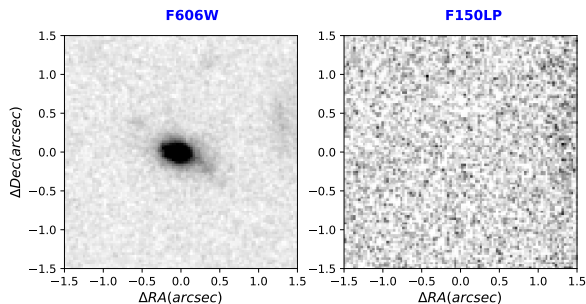

Figure 5. F606W (left) and far-UV F150LP (right) stacked images of our 7 targets. We find no detection of LyC flux in the stacked image either.

random lines-of-sight to accurately sample the column density and number density distributions of the intervening absorbers.

For this simulation, we adopt the number density and column density distributions of the intervening absorbers from the literature (Janknecht et al. 2006; Rao et al. 2006; Ribaudo et al. 2011; O'Meara et al. 2013) as explained in detail in Alavi et al. (2014). We then take the mean IGM absorption from 300 LOSs for each redshift. The IGM absorption value that we used for each galaxy is listed in Table 2.

$(L_{1500}/L_{LyC})^{int}$: This intrinsic flux density ratio depends on the age, star formation history, metallicity and IMF. Ideally, we would fit each individual SED with a stellar population model and derive the intrinsic flux decrement across the Lyman break. However as shown in Siana et al. (2010), the precise SFH is ambiguous and the best-fit SEDs from different SFHs give very different predictions of the intrinsic LyC flux. This is mainly because the portion of SED to which we are fitting the photometry is dominated by stars with ages > 100 Myr, whereas

the LyC flux comes from massive stars with ages < 10 Myr. Relatedly, Rutkowski et al. (2016) argue that for a given star formation history, the largest uncertainty in this intrinsic flux ratio is introduced by the ignorance of the stellar age and the IMF. They further show that this flux ratio can even be affected by stellar rotation and the choice of stellar template libraries. In addition, as discussed in Steidel et al. (2018), depending on the assumed age, metallicity, SFH, IMF and the effect of binary evolution of massive stars, stellar population models predict a range of $0.15 < (L_{900}/L_{1500})^{int} < 0.75$.

Here, we perform a simple analysis to quantify this ratio. We use BC03 (Bruzual & Charlot 2003) stellar population synthesis models with Chabrier IMF, constant SFH and metallicity of $Z = 0.2~Z_{\odot}$. We then derive the UV luminosity at two wavelengths: the ionizing continuum at 700 Å (i.e., the effective wavelength of the F150LP filter used in our SBC imaging) and non-ionizing UV at 1500 Å for a range of ages at [2 Myr, 5 Myr, 10 Myr, 30 Myr, 50 Myr, 100 Myr, 150 Myr, 200 Myr, 500 Myr, 1 Gyr], as shown in Figure 6. At each age, following Inoue (2011), we derive the Hα fluxes and thus the Hα EWs as below:

$$L_{H\beta} = 4.78 \times 10^{-13} \frac{1 - f_{\mathrm{esc,abs}}}{1 + 0.6 f_{\mathrm{esc,abs}}} N_{\mathrm{LyC}} \tag{3}$$
$$L_{H\alpha} = 2.78 \times L H_{\beta}$$

which results from the assumption of Case B recombination (Osterbrock & Ferland 2006). The factors in these equations are calculated by assuming a temperature $T = 10^4$ K and an electron density $n_e = 10^2$ cm^{-3}. N_{LyC} represents the stellar production rate of ionizing photons in units of s^{-1}. The Hα EW values are displayed on the x-axis in Figure 6. The galaxies in the sample have Hα EWs between 190-500 Å as shown in the orange area in Figure 6. We note that we are assuming a constant SFH here, while an instantaneous SFH would result in the same EW range at younger ages (Leitherer et al. 1999; Amorín et al. 2015). From this figure, we see that a $(L_{1500}/L_{\mathrm{LyC}})^{int}$ ratio between 6 and 10 is required to reproduce the observed EW distribution with reasonable assumptions about the escape fraction. In what follows we use the average value of 8, which is consistent with the values used in some of the previous studies including Siana et al. (2007) and Rutkowski et al. (2016).

Following equations 1 and 2 and assuming an intrinsic ratio of 8, we estimate the $f_{\mathrm{esc,rel}}$ values as listed in Table 2. In addition, we also calculate the $f_{\mathrm{esc,abs}}$ values because several studies in the literature report their findings in terms of this quantity. To estimate this quantity, we use the relation of $f_{\mathrm{esc,abs}} = 10^{-0.4 A_{1500}} f_{\mathrm{esc,rel}}$, as described in detail in Siana et al. (2007). Assuming a SMC curve, we derive the dust attenuation at 1500 Å, A_{1500}, using the A$_v$ estimates (see Table 1) from our SED fitting. The $f_{\mathrm{esc,abs}}$ values are listed in Table 2.

As described above, our determination of the escape fraction uses the Hα EW to estimate the $(L_{1500}/L_{\mathrm{LyC}})^{int}$ ratio with an assumed SFH. However, the assumptions made in this analysis could affect our estimate of the $(L_{1500}/L_{\mathrm{LyC}})^{int}$ ratio, and thus the LyC escape fraction values. For example, Siana et al. (2007) shows

that assuming an instantaneous SFH will increase the $(L_{1500}/L_{\mathrm{LyC}})^{\mathrm{int}}$ ratio at a given age. We also note that accounting for the binary evolution of massive stars will decrease this ratio, as it enhances the late-time ionizing photon production (Steidel et al. 2018; Fletcher et al. 2019). Another important uncertainty is the effect of older stellar populations in our interpretation of Hα EW. If there is an extremely young and strong burst of star formation on top of an older stellar population from previous bursts, then the Hα EW will not be as high as expected. This is because the older stellar populations dominate the rest-optical continuum and thus lower the Hα EW. To avoid this uncertainty, we can take the f_{1500} out of the equation and calculate the absolute LyC escape fraction directly from Hα luminosity. If we assume that LyC escape fraction is small, which is a reasonable assumption for our sample, we can then derive the total intrinsic LyC luminosity from the Hα luminosity assuming that all ionizing photons are absorbed and converted to Hα emission line via recombination. We use the above BC03 models and compute the conversion from Hα luminosity to LyC luminosity to be:

$$L_{700} \ [\mathrm{erg \ s^{-1} \ Hz^{-1}}] = 1.7 \times 10^{14} L_{H\alpha} \ [\mathrm{erg \ s^{-1}}] \quad (4)$$

We calculate the Hα luminosity, $L_{H\alpha}$, of our sample by correcting the observed Hα fluxes for dust attenuation assuming an SMC curve. We then use the above equation to derive the intrinsic LyC luminosity, L_{700}, for each galaxy in our sample. Finally, we calculate the $f_{esc,abs}$ values using the ratio of the observed LyC flux limits corrected for the IGM absorption and the intrinsic L_{700} values from equation 4. We report these new estimates of $f_{esc,abs}$ in Table 2. These new values are in general agreement with our original $f_{esc,abs}$ estimates.

As explained before in Section 2.2, we observed each galaxy in our sample with a different depth, which was calculated using the online HST Exposure Time Calculator to reach a 3σ limit for $f_{esc,abs}$ of 5%. Our measured $f_{esc,abs}$ values are consistent with our predicted limits.

5. DISCUSSION

5.1. *Comparison with Other Studies: Physical Properties (SED fitting)*

Given the low success rate of identifying LyC leakers at various redshifts, it is important to compare our sample with other samples and investigate the LyC escape fraction in the context of different physical properties of galaxies.

The photometry of our sample results from a combination of ground- and space-based imaging. This includes 44 and 40 broad photometric bands from near-UV ($\lambda_{rest} \sim 0.19 \ \mu m$) to IRAC4 ($\lambda_{rest} \sim 3.5 \ \mu m$) in COSMOS and GOODS-South fields, respectively. The 3D-HST catalogs provide the best SED fitting parameters for these galaxies, but they assume a metallicity of 1.0 $Z_\odot$. However, the low stellar masses (i.e., $\log(M^*/M_\odot) \sim 9-10$) of our sample suggest lower values of $[0.2, 0.4] \ Z_\odot$ for the metallicity (Wuyts et al. 2012). We perform our own SED fitting using the FAST code (Kriek et al. 2009) on BC03 stellar population models assuming a Chabrier IMF (Chabrier 2003). We assume an exponentially-increasing star formation history (i.e.,
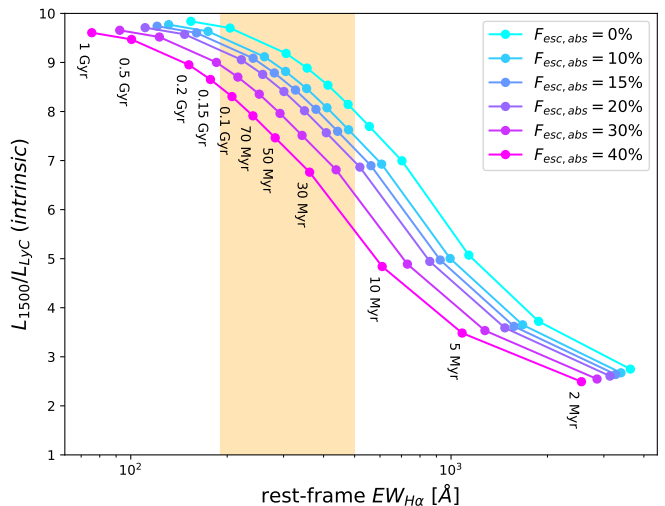

Figure 6. The $(L_{1500}/L_{\mathrm{LyC}})^{\mathrm{int}}$ intrinsic flux ratio as a function of rest-frame Hα EW using the BC03 models with $Z = 0.2 \ Z_\odot$ and constant SFH. Each color specifies a different $f_{esc,abs}$ value as listed in the figure. The Hα EW of galaxies in the observed sample would be located in the shaded orange region.

SFH $\propto e^{t/\tau}$) with $7 < \log(\tau) < 10$, as argued in Reddy et al. (2012) for high-redshift galaxies. We allow the metallicity to change between two values $[0.2, 0.4] \ Z_\odot$. We also select a SMC extinction curve (Gordon et al. 2003) with a range of $0 < A_V < 4$. Some recent studies (Bouwens et al. 2016; Reddy et al. 2018) demonstrate that $z = 1.5 - 2.5$ galaxies have an $IRX - \beta$ relation that is consistent with a steep extinction curve similar to SMC. In addition, we correct the broadband photometry for the contamination from nebular emission lines using the fluxes measured from the 3D-HST spectra. We note that the stellar mass estimates from our SED fitting are close to the 3D-HST stellar masses that we used for our initial sample selection. However, other parameters such as dust attenuation snd SFR have significantly changed.

We compare the stellar masses (M_*), dust reddening parametrized as E(B-V), SFR and specific star formation rate (sSFR = SFR/M^*) of the galaxies in our sample with the quantities of confirmed LyC emitters from other studies. We divide the known LyC emitters in two groups of low $z < 0.4$ and high redshift $z > 2.0$ galaxies. We note that we scale the SFR and sSFR measurements to the Salpeter IMF (Salpeter 1955) for a fair comparison (i.e., multiplying our SFR estimates by a factor of 1.75). Caution must be taken when comparing SFR and color excess with other studies, because these parameters strongly depend on the dust attenuation models. For example, assuming a flat dust curve like Calzetti et al. (2000) would result in a larger value of E(B-V). Therefore, for the comparisons of E(B-V) and SFR values, we only include the studies that use a similar extinction curve (i.e., SMC). In addition, to be consistent with our SFR estimate from the SED fitting, we only compare with the high-redshift studies that use an indicator sensitive to recent SFR (i.e., $\sim 100 \ \mathrm{Myr}$) in galaxies (Mostardi et al. 2015; Shapley et al. 2016; Vanzella et al. 2016; Bian et al. 2017; Naidu et al. 2017; Vanzella et

Table 2
Summary of LyC measurements

ID	U [AB]	$f_{1500}[\mu Jy]$	f_{LyC}[a]$[\mu Jy]$	IGM transmission $(\exp(-\tau))$	$f_{\mathrm{LyC}}/f_{1500}$[b]	$f_{esc,rel}$[c]	$f_{esc,abs}$[d]	$f_{esc,abs}$ [e]
cosmos-1-111	23.68	1.23	< 0.015	0.56	< 0.023	< 0.18	< 0.08	< 0.11
cosmos-3-69	23.73	1.16	< 0.011	0.56	< 0.019	< 0.15	< 0.04	< 0.06
cosmos-3-113	24.11	0.83	< 0.012	0.56	< 0.027	< 0.22	< 0.06	< 0.13
cosmos-13-80	23.95	0.96	< 0.008	0.61	< 0.015	< 0.12	< 0.03	< 0.04
cosmos-28-132	24.20	0.76	< 0.008	0.56	< 0.020	< 0.16	< 0.07	< 0.06
goodss-6-124	24.10	0.83	< 0.007	0.61	< 0.014	< 0.11	< 0.07	< 0.08
goodss-27-124	24.16	0.78	< 0.006	0.61	< 0.012	< 0.10	< 0.06	< 0.04
stacks	...	6.54	< 0.033.	0.60	< 0.009	< 0.07	< 0.06	...

[a] The LyC fluxes are 3σ limits.
[b] This ratio is corrected for the IGM absorption.
[c] An intrinsic ratio of $L_{1500}/L_{\mathrm{LyC}} = 8$ is assumed.
[d] These values are derived from adding dust correction to the $f_{esc,rel}$ values.
[e] These values are derived directly from an estimate of intrinsic LyC luminosity using the Hα luminosity.
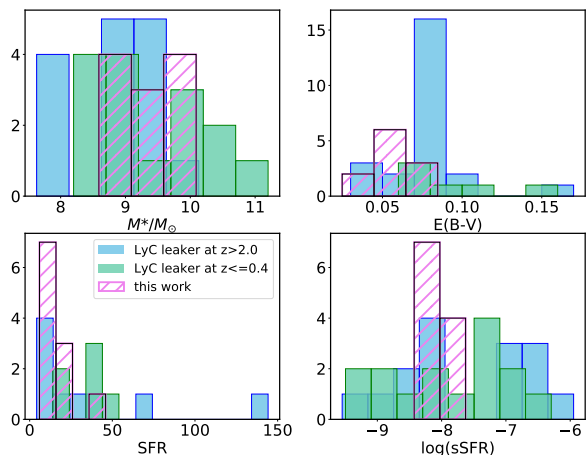

Figure 7. Histograms of the SED fit parameters of M$_*$, color excess E(B-V), SFR and sSFR. The confirmed LyC leakers from literature are shown in blue and green colors for galaxies at $z > 2.0$ and $z < 0.4$, respectively. The parameter distributions of the galaxies in our sample are shown in hashed pink histograms. These galaxies span a similar range of galaxy physical parameters as the other LyC emitters in the literature.

2018; Fletcher et al. 2019). However at low redshifts, we do not find recent SFR measurements corrected with the SMC curve in the literature. To compare with studies at $z < 0.4$, we use their SFR values obtained from extinction-corrected Hβ flux densities reported in Izotov et al. (2016a,b, 2018b,a). We note that SFRs from nebular emission lines trace the star formation activity on timescales of 10 Myr.

Figure 7 compares the distributions of 4 SED parameters of our non-detections (pink hashed histogram) and the corresponding distributions of the other LyC leakers at low (green histogram) and high (blue histogram) redshifts. As seen in the upper-left panel of this figure, the stellar mass distribution of our non-detections overlaps with the stellar mass range covered by the LyC leakers at low and high redshifts. The mean value of our stellar mass distribution $< M^*/M_\odot >= 9.5$ is halfway between the corresponding mean values of $< M^*/M_\odot >= 10$ and $< M^*/M_\odot >= 9.1$ for the LyC leakers at low and high redshifts, respectively.

We also examine the distribution of dust attenuation, E(B-V), in the upper-right panel of Figure 7. The dust distribution of our non-detections overlaps with the lower end of the dust distributions for the LyC emitters.

Finally, as shown in the lower panels of Figure 7, both SFR and sSFR histograms are consistent with the corresponding histograms of the LyC emitters. We should reemphasize that the SFR of low redshift LyC galaxies is derived from the Hβ emission line and thus it estimates the instantaneous SFR, while SFR estimates of our non-detections and high-redshift LyC galaxies are averaged over a timescale of ~ 100 Myr.

In summary, although the confirmed LyC emitters cover a wide range of values for the physical properties discussed above, our measured values do fall within these observed distributions. Our observations demonstrate clearly that none of these parameters, alone, can guarantee a LyC-emitting galaxy.

In Figure 8, we show the observed ratio of $f_{\mathrm{LyC}}/f_{1500}$ corrected for the IGM absorption versus stellar mass (left) and UV absolute magnitude (right) measured at 1500 Å, M_{1500}. The quantity shown on the y-axis is the same as $(f_{\mathrm{LyC}}/f_{1500})^{\mathrm{out}}$ used in equation 2. To ensure a fair comparison between these studies and to bring them to the same framework of IGM transmission estimates, we take the value of the observed ratio (or the 3σ limit) from each paper and correct for IGM absorption by adopting the correction factors at the relevant wavelength from our IGM simulations.

In these plots, we collected measurements of the LyC flux at different redshifts. The confirmed LyC detections are represented in two groups of high-redshift sources at $z > 2$ shown with colored circles (Mostardi et al. 2015; Shapley et al. 2016; Vanzella et al. 2016; Bian et al. 2017; Naidu et al. 2017; Steidel et al. 2018; Vanzella et al. 2018; Fletcher et al. 2019) and low-redshifts sources at $z < 0.4$ shown with colored squares (Leitet et al. 2013; Borthakur et al. 2014; Izotov et al. 2016a,b, 2018b). We also include the non-detection 3σ limits from studies of LyC candidates at $z > 1.0$ (Siana et al. 2007; Cowie et al. 2009; Bridge et al. 2010; Siana et al. 2010; Nestor et al. 2013; Amorín et al. 2014; Siana et al. 2015; Guaita et al. 2016; Grazian et al. 2016; Rutkowski et al. 2016; Marchi et al. 2017; Hernandez et al. 2018; Naidu et al. 2018; Smith et al. 2018). Our 3σ limits (black downward arrows) are lower than the ratio measured for the confirmed LyC
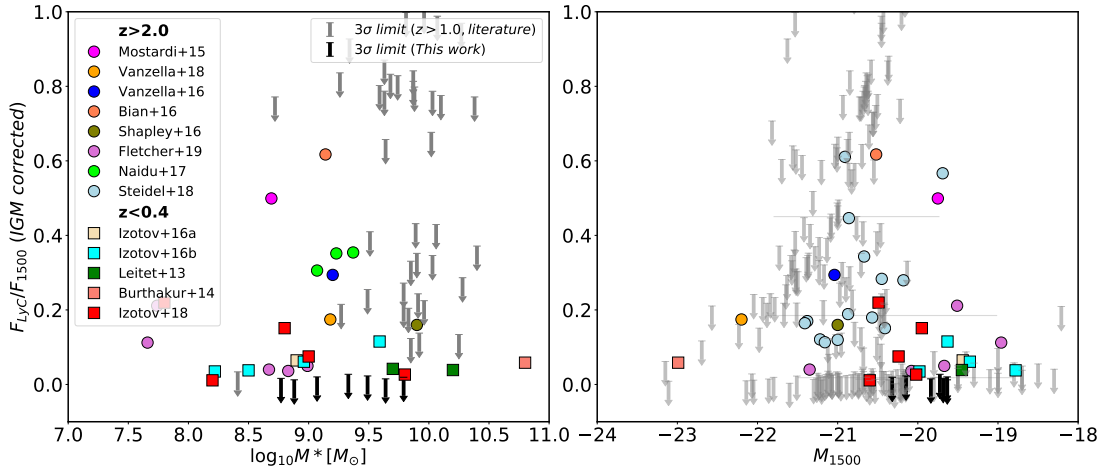
Figure 8. Left: The observed ratio of $f_{\rm LyC}/f_{1500}$ corrected for IGM absorption as a function of stellar mass. The LyC emitters from the literature are shown with colored circles and squares for galaxies at $z > 2$ and $z < 0.4$, respectively, as listed in the figure. Our 3σ non-detection limits are shown as black arrows. Right: The y-axis is similar to the left panel and the x-axis displays the UV absolute magnitude measured at 1500 Å. For both panels, the 3σ non-detections from the literature are from Siana et al. (2007); Cowie et al. (2009); Bridge et al. (2010); Siana et al. (2010); Nestor et al. (2013); Amorín et al. (2014); Siana et al. (2015); Grazian et al. (2016); Guaita et al. (2016); Rutkowski et al. (2016); Marchi et al. (2017); Hernandez et al. (2018); Naidu et al. (2018); Smith et al. (2018). While the galaxies in our sample occupy the same range of M_* and M_{1500}, their flux ratio limits are lower than the ratio observed for LyC leakers.

leakers at higher and lower redshifts. Considering that the galaxies investigated in this study have similar physical properties to the LyC leakers and thus likely the same intrinsic LyC production, our low ratio of $(f_{\rm LyC}/f_{1500})^{\rm out}$ is likely related to the conditions in the ISM, such as high HI column density, and geometrical distribution of dust and neutral gas, which makes it difficult for photons to escape.

5.2. *Comparison with Other Studies: Hα and [OIII] EWs*

Galaxies with intense rest-frame optical emission lines, EW (Hα and/or [OIII]) > 100 Å, are known as "Extreme Emission Line Galaxies" (EELG; see Atek et al. 2011). At the wavelengths of these nebular emission lines, the EW is indicative of the ratio of current SFR -thus numerous hot O-type stars producing ionizing LyC photons- to the integrated past SFR. Therefore, EELGs are undergoing a starburst episode with a significant population of new stars. Relatedly, Amorín et al. (2015) demonstrate that these galaxies are dominated by young (< 10 Myr) star-forming regions. In a recent work, Reddy et al. (2018), using an extensive spectroscopic survey of star-forming galaxies at $z = 1.4 - 3.8$, show that high-EW galaxies, especially those with high [OIII] EW, have both high ionization parameter and ionizing photon production rate (i.e, ξ_{ion}). A more recent study by Tang et al. (2019) shows similar results. These characteristics have made EELGs ideal objects in which to search for escaping ionizing photons.

In addition, some studies (Henry et al. 2015; Yang et al. 2017) discovered that $\sim 70\% - 100\%$ of Green Peas, EELGs with high [OIII] EW at low-redshift, are strong Lyα emitters. Using Lyα radiative transfer simulations, Verhamme et al. (2015) have argued that the detection of Lyα in emission from galaxies can be used to identify LyC emitters. Specifically, Lyα profiles can be indicative of LyC-leaking star clusters. They show a

Lyα spectrum with either an asymmetric redshifted profile with small shift or non-zero Lα flux blue-ward of the systematic redshift can be an indicator of escaping LyC photons. In addition, some observational studies such as Steidel et al. (2018) and Fletcher et al. (2019) found high LyC escape fraction for Lyα emitters. This is another piece of evidence that EELGs are likely to be LyC emitters.

The incidence of galaxies with high EW of emission lines (either Hα or [OIII] with rest-frame EW > 100 Å) in the currently available sample of LyC leakers at low redshifts (Izotov et al. 2016a,b, 2018b,a) and high redshifts (Vanzella et al. 2016; Naidu et al. 2017; Vanzella et al. 2018; Fletcher et al. 2019), suggests that high EW nebular emission lines may be a potential indirect tracer of a high escape fraction of ionizing photons. We investigate this by comparing the distribution of Hα (and [OIII]) EWs of the confirmed LyC emitters and the non-detections including EELGs in this study.

Our sources are selected to have strong Hα emission lines and they cover the EW range between $EW_{H\alpha} = 190 - 500$ Å. They also have intense [OIII] emission lines with rest-frame $EW_{[OIII]} = 50 - 740$ Å. As explained in detail in section 4, we do not detect significant ionizing flux in either the individual galaxies or the stack. This is not the first time that observations of EELGs have not detected escaping LyC photons (e.g., Rutkowski et al. 2016; Naidu et al. 2018). Figure 9 compiles the LyC measurements, detections and non-detections, where an estimate of Hα and/or [OIII] EW is available. It shows the IGM corrected $f_{\rm LyC}/f_{1500}$ as a function of [OIII] EW in the left panel and Hα EW in the right panel.

[OIII] EW: As seen in the left panel in Figure 9, galaxies in our sample (black arrows) span a wide range of rest-frame [OIII] EW similar to the confirmed LyC leakers at lower and higher redshifts (Leitet et al. 2013; Naidu et al. 2017; Fletcher et al. 2019; Rivera-Thorsen et al. 2019).
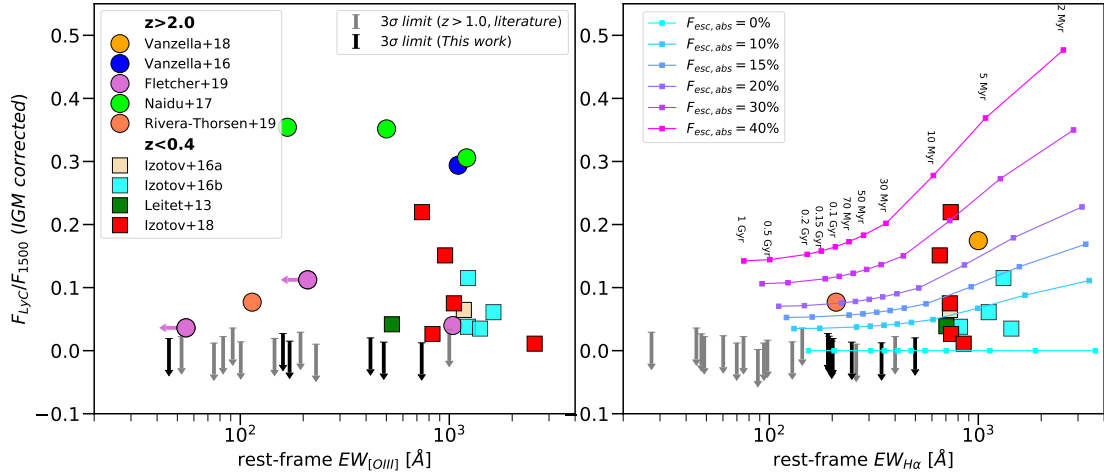
Figure 9. Left: The y-axis is similar to Figure 8 and the x-axis shows the rest-frame [OIII] EW. Right: Similar to the left panel with the x-axis values representing the Hα EW. For both panels, the 3σ non-detections from the literature are from Amorín et al. (2014); Rutkowski et al. (2016); Hernandez et al. (2018); Naidu et al. (2018). The targets in the current work have a distribution of [OIII] EW that is similar to the distribution observed in LyC leakers. This conclusion is less clear for the Hα EW, where the detections have nominally higher Hα EW values. One possibility is that the sample of LyC emitters with Hα EW measurement is somewhat incomplete due to lack of observations of the Hα line at $z > 2.5$, where most of the high-redshift LyC emitters are. The solid lines in the right panel are obtained from our simple BC03 models, which predict the value of $(f_{\rm LyC}/f_{1500})^{\rm out}$ at ages varying between 2 Myr and 1 Gyr for a range of LyC escape fraction assumptions.
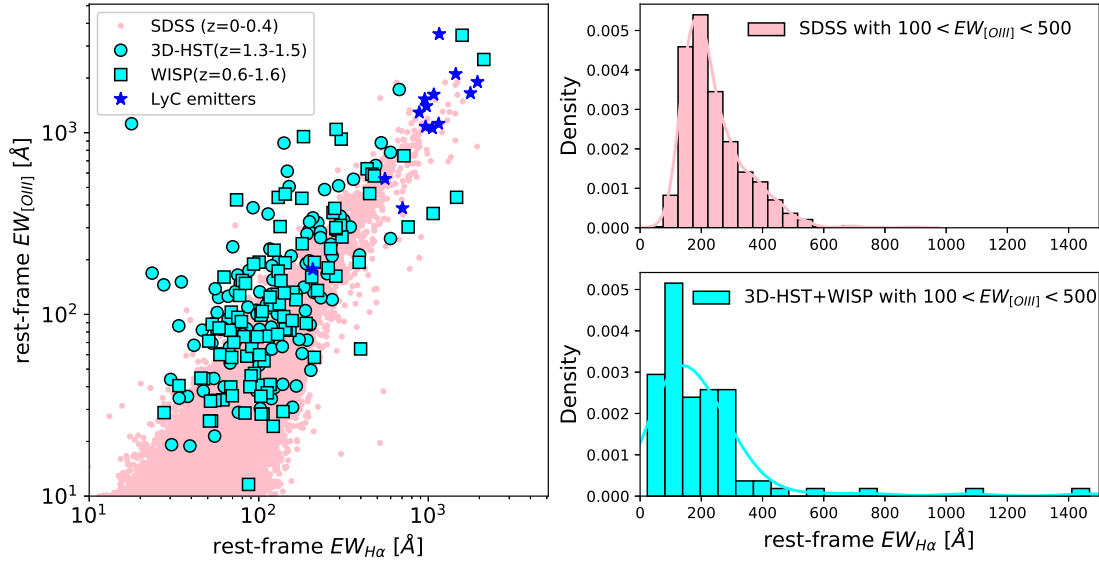

Figure 10. Left: This plot compares the rest-frame Hα and [OIII] EW values of galaxies at $1.3 < z < 1.5$ in the 3D-HST survey. The correlation seen between these two quantities allows us to predict the Hα EW of the medium-intensity [OIII] emitters. Right (top): The distribution of Hα EW of SDSS galaxies with moderate [OIII] EW of $100 < EW < 500$. Right (bottom): The distribution of Hα EW of 3D-HST+WISP galaxies with moderate [OIII] EW of $100 < EW < 500$. Both histograms peak around medium values of Hα EWs and they do not cover extreme vales of $\sim > 600$Å.

However, our sample does not cover the very extreme EW values (i.e., [OIII] EW > 1000 Å) seen in some of the LyC emitters at low (Izotov et al. 2016b, 2018b,a) and high redshift (Vanzella et al. 2016). This plot re-confirms the conclusion presented in previous studies (Izotov et al. 2017; Naidu et al. 2017; Fletcher et al. 2019) that high [OIII] EW on its own is an insufficient diagnostic tool for the leakage of LyC photons.

Hα EW: In the right panel of Figure 9, we investigate the possibility of a correlation between detecting LyC photons and the EW of the Hα nebular emission line. Unfortunately, there are not many high-redshift LyC emitters for which a measurement of Hα EW is available. One galaxy at $z = 4$ from Vanzella et al. (2018)

[11] and one galaxy at $z = 2.4$ from Rivera-Thorsen et al. (2019) are the only high-redshift LyC emitters with Hα EW measurements. Therefore, any conclusion based on their small number should be used with caution. We note that among all of the high-redshift LyC leakers in the literature, more than 90% are at $z > 3$ where an estimate of the Hα EW is very challenging.

Our sample with moderate Hα EW at EW$_{H\alpha}$ = $190 - 500$ Å spans the same range of rest-frame Hα EW as some of the non-detections in the literature (Siana et al. 2010; Rutkowski et al. 2016; Hernandez et al. 2018; Naidu et al. 2018). The Hα EW of a confirmed LyC emitter at $z = 2.37$ by Rivera-Thorsen et al. (2019) is also within this range. In contrast, the group of confirmed LyC emitters (filled squares and orange circle in the right panel of Figure 9) with extreme Hα EWs including several low-redshift sources at $z < 0.4$ and only one high-redshift galaxy (*ion3* at $z = 4$ from Vanzella et al. 2018), looks to be separated from the non-detected sources at moderate Hα EWs. In what follows, we first suggest two scenarios that can explain the lack of LyC emitters seen at moderate Hα EWs. We then investigate whether Hα EW is an effective proxy for LyC emissivity.

5.2.1. *Moderate Hα EW*

As mentioned above, while searches for emerging LyC photons have yielded null results (except the study by Rivera-Thorsen et al. 2019) for galaxies with moderate Hα EWs, galaxies with extreme Hα EWs usually seem to be LyC emitters. This dichotomy (see the right panel of Figure 9) could be due to small number statistics. However, if the dichotomy is real, it could suggest that sources with moderate intensity Hα emission have a lower LyC escape fraction than that of the sources with extreme Hα EW. Below, we discuss these two scenarios.

First Scenario: We show that a moderate Hα EW does not necessary imply a null LyC emissivity, and thus the dichotomy seen in Figure 9 might be due to small number statistics. As pointed out before, the number of confirmed high-redshift LyC emitters with Hα EW measurements available is only two compared to the eight high-redshift LyC emitters with [OIII] EW measurements discussed above. Here, we perform a validation experiment to predict the Hα EWs of those LyC emitters without Hα line measurements and to investigate if any of them are likely to have moderate Hα EW.

We select 3D-HST galaxies at $1.3 < z < 1.5$, where both Hα and [OIII] emission lines are available. We re-measure the EW values of these two lines, because the 3D-HST catalogs have been reported to overestimate the EWs when the continuum detected by the grism is faint (Naidu et al. 2017). In addition, we include galaxies from the WFC3 Infrared Spectroscopic Parallel Survey (WISP, Atek et al. 2010). The WISP survey obtained slitless near-IR grism spectroscopy of more than 200 independent fields in pure-parallel mode with WFC3. This survey observes both Hα and [OIII] emission lines for galaxies at $0.6 < z < 1.6$. For comparison, we also include a sample of $\sim 100,000$ local galaxies at $z < 0.4$

drawn from the Sloan Digital Sky Survey (SDSS, York et al. 2000) DR12 release (Alam et al. 2015).

As shown in the left panel of Figure 10, the Hα and [OIII] EWs strongly correlate such that we do not expect extreme Hα EW (i.e., ¿ 600 Å) for moderate-intensity [OIII] lines (i.e., $100 < $ EW$_{[OIII]} < 500$). To further investigate this quantitatively, we plot the distribution of Hα EW values for a range of moderate [OIII] EW values of $100 < $ EW$_{[OIII]} < 500$ for SDSS and 3D-HST+WISP galaxies in the upper-right and lower-right panels of Figure 10, respectively. As seen in these histograms, galaxies with moderate [OIII] EW values are very likely to be moderate Hα emitters. Therefore, those LyC emitters with moderate [OIII] EW values (e.g., purple and light green circles in the left panel of Figure 9) and no Hα line measurement, are presumably moderate Hα emitters as well.

We should note that the [OIII] emission line is sensitive to the presence of very young hot stars. Hα is instead sensitive to the presence of somewhat less extreme photons (i.e., 13.6 eV). Therefore, for a given moderate-intensity [OIII] line, it is theoretically possible to obtain an extreme Hα EW. However, as seen in Figure 10, observational values from SDSS, 3D-HST and WISP surveys do not show many of such examples, and thus they must be rare.

In addition, we over-plot the LyC emitters (blue stars) from literature in the left panel of Figure 10. As illustrated in this figure, the currently known LyC emitters follow the mean relation between the [OIII] and Hα EWs seen in the SDSS, 3D-HST and WISP galaxies. Therefore, it is likely that the absence of moderate Hα emitters is just a selection effect.

Finally, we would like to emphasize that this scenario and its conclusion are solely based on the prediction of Hα EW values, and a definitive answer requires direct measurement of Hα emission lines for the LyC emitters with moderate [OIII] EWs.

Second Scenario: The lack of galaxies with high LyC emissivity at moderate Hα EWs may be indicative of a real relation. To further investigate this possibility, we use our simple models (as described in Section 4.3) to understand how the observed ratio of f_{LyC}/f_{1500} changes with Hα EW. We calculate the observed f_{LyC}/f_{1500} ratios in our models by applying a range of assumed escape fraction values, $f_{esc,abs} = [0\%, 10\%, 20\%, 30\%, 40\%]$, to the intrinsic f_{LyC}/f_{1500} ratios calculated in Section 4.3. To be consistent with the observed ratios of the real galaxies, we also add the effect of dust attenuation at LyC and 1500 Å wavelengths, using a median of the color excess values, E(B-V), of all the LyC emitters in the literature. As illustrated in the right panel of Figure 9, the observed ratios are calculated at different ages, ranging from 2 Myr to 1 Gyr, corresponding to different Hα EWs.

The lines seen in the right panel of Figure 9 are the results of variation of age and LyC escape fraction in the models. The age parameter is changing in the direction of the x-axis such that stellar populations are aging as we move along these lines toward lower Hα EWs. On the other hand, the LyC escape fraction parameter causes the spread in the direction of the y-axis. Based on our simple models, we can think of galaxies with moderate Hα EWs to be similar to galaxies with extreme Hα EWs

---

[11] It should be noted that the EW measurement for this redshift is not from spectroscopic data. Using its broad-band photometry and a clear excess in the 3.6μm flux, they estimate a rest-frame Hα EW of 1000 Å.

but with older ages. Therefore, if we assume that the distribution of LyC escape fraction at moderate Hα EWs is the same as the distribution seen at extreme Hα EWs, then we would expect to detect some LyC emitters at lower Hα EWs. Because we do not detect any LyC emission at these moderate Hα EWs, we can conclude that the LyC escape fraction in older galaxies (i.e., with moderate Hα EWs) must be lower.

In conclusion from the two scenarios described above, whether the lack of LyC emitters at moderate Hα EWs is due to small number statistics (i.e., first scenario in which we could see both LyC emitters and non-detections) or having a lower LyC escape fraction (i.e., second scenario in which we mostly see non-detections), moderate Hα EW, alone, is not a promising indicator of lyC leakage.

5.2.2. *Extreme Hα EW*

With the currently available data (i.e., finding only LyC emitters and no non-detections at extreme Hα EWs), we can suggest that an extreme Hα emission (i.e., Hα EW $\sim 600 - 1000$ Å and beyond) is likely an effective tracer of LyC emissivity.

However, we would like to note the work by Izotov et al. (2017) who indirectly derive the LyC escape fraction of a sample of local compact star-forming galaxies with extreme Hα and [OIII] emission lines. They investigate whether the galaxies in their sample can emit LyC by constraining their neutral gas column densities through photoionized H II region models. For two out of five of the galaxies in their sample with extreme Hα emission (Hα EW ~ 2000 Å, private communication), they derive a high neutral gas column density, implying a negligible LyC escape fraction. In case of a direct observation, this negligible LyC escape fraction would likely result in null LyC emissivity. This would contradict our suggestion that an extreme Hα emitter is likely a LyC leaker. More definite conclusion about these sources will require a direct observation of their LyC emission.

Finally, we should emphasize that the above discussions ignore the effect of redshift evolution on the properties of LyC emitters. As seen in Figure 9, all of the low-redshift LyC emitters have extreme [OIII] and Hα EWs (i.e., > 600 Å), while the high-redshift LyC emitters cover a wider range of EW values. A deeper understanding of possible redshift evolution requires a larger sample of confirmed LyC emitters at various redshifts.

5.3. *Understanding the Non-detections*

Our SED fits show that the physical properties (stellar mass, SFR and dust attenuation) of the galaxies in our sample are similar to those of the confirmed LyC emitters. However, the galaxies in our sample have lower Hα EWs than almost all of the LyC emitters with Hα line measurements in the literature (with an exception of a study by Rivera-Thorsen et al. 2019). A direct interpretation of our results is that the galaxies in our sample are older and thus they are likely to have lower LyC escape fraction (see Section 5.2 and the right panel of figure 9). This simple interpretation explains why we did not detect escaping LyC emission in this study.

The above interpretation simply explains our non-detections in comparison with the LyC emitters with measured Hα EWs as seen in Figure 9. However, we

saw (see Section 5.2.1) that this plot is probably more complicated than it looks. To further understand our non-detections in the context of these possible complications, we discuss other scenarios below.

While LyC emitters with Hα line measurements have extreme Hα EWs, we showed that LyC emitters with moderate Hα EWs possibly exist as well (see Section 5.2.1). If we accept such a possibility, we need to understand why the galaxies in our sample, with Hα EWs similar to those possible LyC emitters, have low LyC emissivity.

Because the stellar populations, and thus the LyC photon production of the galaxies in our sample and those possible LyC emitters at moderate Hα EWs are the same, the non-detections in our sample must be a result of the LyC photons not being able to escape. To further understand this, we consider a scenario suggested by hydrodynamical simulations (Cen & Kimm 2015; Ma et al. 2015; Paardekooper et al. 2015), in which the ionizing photons escaping from galaxies into the IGM are highly anisotropic. Consequently, as also noted in Paardekooper et al. (2015), even if the galaxies in our sample have high *actual* escape fraction, there can be many sight lines through which no ionizing radiation escapes. Therefore, our results strongly depend on the orientation of the galaxies. This emphasizes the importance of including large samples in the observational studies.

We note that the direction dependency of LyC escape fraction seems to be more significant at lower Hα EWs than is at extreme Hα EWs. As seen in Figure 9, all LyC searches at extreme Hα EWs resulted in LyC detections and there is no non-detections at these extreme EWs, in contrast to what we would expect for an anisotropic distribution of escaping LyC emission. To better understand this conflict, we consider a "picket fence" model in which the neutral gas surrounding the ionizing sources is patchy. In this model where parts of the galaxy are covered with optically thick clouds, LyC photons escape from optically thin holes between the clouds. The distributions of these holes and their sizes likely depend on how strong the galactic feedback is. In an extreme starburst (i.e., extreme Hα EW), strong stellar feedback may effectively expel neutral gas and lower the covering fraction, thus allowing LyC photons to escape more easily in different directions. However in a less extreme condition (i.e., moderate/low Hα EW), the covering fraction is higher and weaker stellar feedback creates random optically thin channels in the ISM (Zackrisson et al. 2013). In this situation, we can detect the LyC photons only if they are emitted in the thin channels directed toward our line of sight.

Future observations of the LyC escape fraction will require a large, representative sample of galaxies. To achieve this goal, effective selection techniques will be vital. As is also discussed in Rutkowski et al. (2016) and Fletcher et al. (2019), we are lacking very low-mass galaxies (i.e., $\log(M_*/M_\odot) < 9$), the so-called dwarf galaxies, in the LyC studies at high redshifts including this study at $z \sim 1$. As suggested in many theoretical studies and most simulations (e.g., Yajima et al. 2011; Wise et al. 2014; Lewis et al. 2020; Ma et al. 2020), these low-mass galaxies likely have a high escape fraction of ionizing photons. For example, a recent work by Ma et al. (2020) predicts that LyC escape fraction increases with stellar

mass up to $M^* \sim 10^8 M_\odot$ and decreases at higher masses. Therefore, a likely path for future studies of LyC escape fraction at $z \sim 1$ is to observe very low-mass dwarf galaxies as promising candidates for escaping ionising radiation.

6. SUMMARY

We have obtained ACS/SBC far-UV imaging of 11 star-forming galaxies at $1.2 < z < 1.4$ to search for escaping LyC emission. We select our targets from the 3D-HST survey to have strong Hα emission lines with EW > 190 Å and low stellar masses with $\log(M_*/M_\odot) < 10$. These criteria identify sources that are undergoing a starburst episode with a significant population of new stars and thus they are ideal to search for escaping ionizing photons. Our findings are as follows.

- After careful data reduction and subtraction of the dark current as the dominant source of noise, we do not detect (i.e., S/N > 3) any escaping LyC radiation from the individual targets or in the stack.

- We run a Monte Carlo simulation (Siana et al. 2010; Alavi et al. 2014) to compute the IGM absorption. This simulation properly accounts for varying opacity of the IGM along different lines of sight. Applying these IGM corrections, we calculate 3σ limits of $f_{\rm LyC}/f_{1500} < [0.014 - 0.027]$ and < 0.009 for the individual galaxies and stack, respectively. Assuming an intrinsic ratio of $(L_{1500}/L_{\rm LyC})^{\rm int} = 8$, these limits translate to 3σ limits of $f_{esc,rel} < [0.10, 0.22]$ and $f_{esc,rel} < 0.07$ for the individual galaxies and stack, respectively.

- We fit stellar population models to the multi-band photometry of our sample covering from rest-frame UV to near-IR to estimate the physical parameters. The galaxies in our sample exhibit similar ranges of stellar mass, SFR and dust attenuation values as the confirmed LyC emitters in the literature. Our findings indicate that none of these galaxy parameters, alone, is a promising indicator of LyC leakage.

- We compare the Hα and [OIII] EW values of our sample and those of the confirmed LyC emitters in the literature. Our Hα and [OIII] EW estimates are in the range of EW$_{rest} \sim [190 - 500]$ Å and $[50 - 700]$ Å, respectively. Our sample does not cover extreme values (i.e., > 600 Å) seen in some of the LyC emitters in the literature (Izotov et al. 2016a,b; Vanzella et al. 2016; Izotov et al. 2018b,a; Vanzella et al. 2018). For [OIII] emission lines, we find that high [OIII] EW values do not guarantee the detection of LyC flux. This conclusion is consistent with the findings from previous studies (Izotov et al. 2017; Naidu et al. 2017; Fletcher et al. 2019). For the Hα emission line, we demonstrate that a moderate EW (i.e., < 600 Å) is not a promising indicator of leaking LyC photons. However, considering current evidence, it is likely that extreme Hα emission (i.e., $\sim 600 - 1000$ Å and beyond) is an effective indicator of LyC leakage.

Future observations of LyC emission may have to combine various indirect selection techniques (i.e., profile of Lyα line, UV spectral slope, ultra-faint dwarf galaxies with very low stellar mass) to better identify LyC emitters at of $z \sim 1$.

REFERENCES

Alam, S., Albareti, F. D., Allende Prieto, C., et al. 2015, ApJS, 219, 12

Alavi, A., Siana, B., Richard, J., et al. 2014, ApJ, 780, 143

—. 2016, ApJ, 832, 56

Amorín, R., Grazian, A., Castellano, M., et al. 2014, ApJ, 788, L4

Amorín, R., Pérez-Montero, E., Contini, T., et al. 2015, A&A, 578, A105

Atek, H., Richard, J., Kneib, J.-P., & Schaerer, D. 2018, MNRAS, 479, 5184

Atek, H., Malkan, M., McCarthy, P., et al. 2010, ApJ, 723, 104

Atek, H., Siana, B., Scarlata, C., et al. 2011, ApJ, 743, 121

Avila, R. J. 2017, Updated Measurements of ACS/SBC Dark Rates, Tech. rep.

Bertin, E., & Arnouts, S. 1996, A&AS, 117, 393

Bian, F., Fan, X., McGreer, I., Cai, Z., & Jiang, L. 2017, ApJ, 837, L12

Borthakur, S., Heckman, T. M., Leitherer, C., & Overzier, R. A. 2014, Science, 346, 216

Boutsia, K., Grazian, A., Giallongo, E., et al. 2011, ApJ, 736, 41

Bouwens, R. J., Illingworth, G. D., Oesch, P. A., et al. 2015, ApJ, 811, 140

Bouwens, R. J., Oesch, P. A., Illingworth, G. D., Ellis, R. S., & Stefanon, M. 2017, ApJ, 843, 129

Bouwens, R. J., Aravena, M., Decarli, R., et al. 2016, ApJ, 833, 72

Brammer, G. B., van Dokkum, P. G., Franx, M., et al. 2012, The Astrophysical Journal Supplement Series, 200, 13

Bridge, C. R., Teplitz, H. I., Siana, B., et al. 2010, ApJ, 720, 465

Bruzual, G., & Charlot, S. 2003, MNRAS, 344, 1000

Calzetti, D., Armus, L., Bohlin, R. C., et al. 2000, ApJ, 533, 682

Cardamone, C., Schawinski, K., Sarzi, M., et al. 2009, MNRAS, 399, 1191

Cardelli, J. A., Clayton, G. C., & Mathis, J. S. 1989, ApJ, 345, 245

Cen, R., & Kimm, T. 2015, ApJ, 801, L25

Chabrier, G. 2003, PASP, 115, 763

Cowie, L. L., Barger, A. J., & Trouille, L. 2009, ApJ, 692, 1476

Deharveng, J. M., Buat, V., Le Brun, V., et al. 2001, A&A, 375, 805

Emami, N., Siana, B., Alavi, A., et al. 2020, ApJ, 895, 116

Erben, T., Hildebrandt, H., Lerchster, M., et al. 2009, A&A, 493, 1197

Faisst, A. L. 2016, ApJ, 829, 99

Fan, X., Carilli, C. L., & Keating, B. 2006, Annual Review of Astronomy and Astrophysics, 44, 415

Ferland, G. J., Korista, K. T., Verner, D. A., et al. 1998, PASP, 110, 761

Fletcher, T. J., Tang, M., Robertson, B. E., et al. 2019, ApJ, 878, 87

Ford, H. C., Bartko, F., Bely, P. Y., et al. 1998, in Society of Photo-Optical Instrumentation Engineers (SPIE) Conference Series, Vol. 3356, Space Telescopes and Instruments V, ed. P. Y. Bely & J. B. Breckinridge, 234–248

Giallongo, E., Grazian, A., Fiore, F., et al. 2015, A&A, 578, A83

—. 2019, ApJ, 884, 19

Gordon, K. D., Clayton, G. C., Misselt, K. A., Landolt, A. U., & Wolff, M. J. 2003, ApJ, 594, 279

Grazian, A., Giallongo, E., Gerbasi, R., et al. 2016, A&A, 585, A48

Grimes, J. P., Heckman, T., Aloisi, A., et al. 2009, The Astrophysical Journal Supplement Series, 181, 272

Guaita, L., Pentericci, L., Grazian, A., et al. 2016, A&A, 587, A133

Henry, A., Scarlata, C., Martin, C. L., & Erb, D. 2015, ApJ, 809, 19

Hernandez, S., Leitherer, C., Boquien, M., et al. 2018, MNRAS, 478, 1292

Hildebrandt, H., Pielorz, J., Erben, T., et al. 2009, A&A, 498, 725

Inoue, A. K. 2011, MNRAS, 415, 2920

Inoue, A. K., Shimizu, I., Iwata, I., & Tanaka, M. 2014, MNRAS, 442, 1805

Ishigaki, M., Kawamata, R., Ouchi, M., et al. 2018, ApJ, 854, 73

Iwata, I., Inoue, A. K., Matsuda, Y., et al. 2009, ApJ, 692, 1287

Izotov, Y. I., Guseva, N. G., Fricke, K. J., & Henkel, C. 2016a, MNRAS, 462, 4427

Izotov, Y. I., Schaerer, D., Thuan, T. X., et al. 2016b, MNRAS, 461, 3683

Izotov, Y. I., Schaerer, D., Worseck, G., et al. 2018a, MNRAS, 474, 4514

—. 2020, MNRAS, 491, 468

Izotov, Y. I., Thuan, T. X., & Guseva, N. G. 2017, MNRAS, 471, 548

Izotov, Y. I., Worseck, G., Schaerer, D., et al. 2018b, MNRAS, 478, 4851

Janknecht, E., Reimers, D., Lopez, S., & Tytler, D. 2006, A&A, 458, 427

Jaskot, A. E., & Oey, M. S. 2013, ApJ, 766, 91

Kriek, M., van Dokkum, P. G., Labbé, I., et al. 2009, ApJ, 700, 221

Kulkarni, G., Worseck, G., & Hennawi, J. F. 2019, MNRAS, 488, 1035

Leitet, E., Bergvall, N., Hayes, M., Linné, S., & Zackrisson, E. 2013, A&A, 553, A106

Leitet, E., Bergvall, N., Piskunov, N., & Andersson, B. G. 2011, A&A, 532, A107

Leitherer, C., Ferguson, H. C., Heckman, T. M., & Lowenthal, J. D. 1995, ApJ, 454, L19

Leitherer, C., Hernandez, S., Lee, J. C., & Oey, M. S. 2016, ApJ, 823, 64

Leitherer, C., Schaerer, D., Goldader, J. D., et al. 1999, ApJS, 123, 3

Lewis, J. S. W., Ocvirk, P., Aubert, D., et al. 2020, arXiv e-prints, arXiv:2001.07785

Livermore, R. C., Finkelstein, S. L., & Lotz, J. M. 2017, ApJ, 835, 113

Ma, X., Kasen, D., Hopkins, P. F., et al. 2015, MNRAS, 453, 960

Ma, X., Quataert, E., Wetzel, A., et al. 2020, arXiv e-prints, arXiv:2003.05945

MacKenty, J. W., Kimble, R. A., O'Connell, R. W., & Townsend, J. A. 2010, Society of Photo-Optical Instrumentation Engineers (SPIE) Conference Series, Vol. 7731, On-orbit performance of HST Wide Field Camera 3, 77310Z

Madau, P., & Dickinson, M. 2014, ARA&A, 52, 415

Malkan, M., Webb, W., & Konopacky, Q. 2003, ApJ, 598, 878

Marchi, F., Pentericci, L., Guaita, L., et al. 2017, A&A, 601, A73

Mason, C. A., Trenti, M., & Treu, T. 2015, ApJ, 813, 21

Mason, C. A., Fontana, A., Treu, T., et al. 2019, MNRAS, 485, 3947

Masters, D., Capak, P., Salvato, M., et al. 2012, ApJ, 755, 169

Matsuoka, Y., Strauss, M. A., Kashikawa, N., et al. 2018, ApJ, 869, 150

Matthee, J., Sobral, D., Best, P., et al. 2017, MNRAS, 465, 3637

Momcheva, I. G., Brammer, G. B., van Dokkum, P. G., et al. 2016, ApJS, 225, 27

Mostardi, R. E., Shapley, A. E., Steidel, C. C., et al. 2015, ApJ, 810, 107

Naidu, R. P., Forrest, B., Oesch, P. A., Tran, K.-V. H., & Holden, B. P. 2018, MNRAS, 478, 791

Naidu, R. P., Oesch, P. A., Reddy, N., et al. 2017, ApJ, 847, 12

Nakajima, K., & Ouchi, M. 2014, MNRAS, 442, 900

Nestor, D. B., Shapley, A. E., Kornei, K. A., Steidel, C. C., & Siana, B. 2013, ApJ, 765, 47

Nestor, D. B., Shapley, A. E., Steidel, C. C., & Siana, B. 2011, ApJ, 736, 18

Nonino, M., Dickinson, M., Rosati, P., et al. 2009, ApJS, 183, 244

Oke, J. B., & Gunn, J. E. 1983, ApJ, 266, 713

O'Meara, J. M., Prochaska, J. X., Worseck, G., Chen, H.-W., & Madau, P. 2013, ApJ, 765, 137

Ono, Y., Ouchi, M., Harikane, Y., et al. 2018, Publications of the Astronomical Society of Japan, 70, S10

Osterbrock, D. E., & Ferland, G. J. 2006, Astrophysics of gaseous nebulae and active galactic nuclei

Paardekooper, J.-P., Khochfar, S., & Dalla Vecchia, C. 2015, MNRAS, 451, 2544

Parsa, S., Dunlop, J. S., & McLure, R. J. 2018, MNRAS, 474, 2904

Pelló, R., Hudelot, P., Laporte, N., et al. 2018, A&A, 620, A51

Pentericci, L., Vanzella, E., Fontana, A., et al. 2014, ApJ, 793, 113

Planck Collaboration, Adam, R., Aghanim, N., et al. 2016, A&A, 596, A108

Rao, S. M., Turnshek, D. A., & Nestor, D. B. 2006, ApJ, 636, 610

Reddy, N. A., Pettini, M., Steidel, C. C., et al. 2012, ApJ, 754, 25

Reddy, N. A., Steidel, C. C., Fadda, D., et al. 2006, ApJ, 644, 792

Reddy, N. A., Oesch, P. A., Bouwens, R. J., et al. 2018, ApJ, 853, 56

Ribaudo, J., Lehner, N., & Howk, J. C. 2011, ApJ, 736, 42

Rivera-Thorsen, T. E., Dahle, H., Chisholm, J., et al. 2019, Science, 366, 738

Robertson, B. E., Ellis, R. S., Furlanetto, S. R., & Dunlop, J. S. 2015, ApJ, 802, L19

Robertson, B. E., Furlanetto, S. R., Schneider, E., et al. 2013, ApJ, 768, 71

Rutkowski, M. J., Scarlata, C., Haardt, F., et al. 2016, ApJ, 819, 81

Rutkowski, M. J., Scarlata, C., Henry, A., et al. 2017, ApJ, 841, L27

Salpeter, E. E. 1955, ApJ, 121, 161

Schlafly, E. F., & Finkbeiner, D. P. 2011, ApJ, 737, 103

Shapley, A. E., Steidel, C. C., Pettini, M., Adelberger, K. L., & Erb, D. K. 2006, ApJ, 651, 688

Shapley, A. E., Steidel, C. C., Strom, A. L., et al. 2016, ApJ, 826, L24

Siana, B., Teplitz, H. I., Colbert, J., et al. 2007, ApJ, 668, 62

Siana, B., Polletta, M. d. C., Smith, H. E., et al. 2008, ApJ, 675, 49

Siana, B., Teplitz, H. I., Ferguson, H. C., et al. 2010, ApJ, 723, 241

Siana, B., Shapley, A. E., Kulas, K. R., et al. 2015, ApJ, 804, 17

Skelton, R. E., Whitaker, K. E., Momcheva, I. G., et al. 2014, ApJS, 214, 24

Smith, B. M., Windhorst, R. A., Jansen, R. A., et al. 2018, ApJ, 853, 191

Stark, D. P., Ellis, R. S., Chiu, K., Ouchi, M., & Bunker, A. 2010, MNRAS, 408, 1628

Stasińska, G., Izotov, Y., Morisset, C., & Guseva, N. 2015, A&A, 576, A83

Steidel, C. C., Bogosavlevic, M., Shapley, A. E., et al. 2018, ArXiv e-prints

Steidel, C. C., Pettini, M., & Adelberger, K. L. 2001, ApJ, 546, 665

Tang, M., Stark, D. P., Chevallard, J., & Charlot, S. 2019, MNRAS, 489, 2572

Teplitz, H. I., Siana, B., Brown, T. M., et al. 2006, AJ, 132, 853

Vanzella, E., Siana, B., Cristiani, S., & Nonino, M. 2010, MNRAS, 404, 1672

Vanzella, E., Guo, Y., Giavalisco, M., et al. 2012, ApJ, 751, 70

Vanzella, E., de Barros, S., Vasei, K., et al. 2016, ApJ, 825, 41

Vanzella, E., Nonino, M., Cupani, G., et al. 2018, MNRAS, 476, L15

Vasei, K., Siana, B., Shapley, A. E., et al. 2016, ArXiv e-prints

Verhamme, A., Orlitová, I., Schaerer, D., & Hayes, M. 2015, A&A, 578, A7

Willott, C. J., Delfosse, X., Forveille, T., Delorme, P., & Gwyn, S. D. J. 2005, ApJ, 633, 630

Wise, J. H., Demchenko, V. G., Halicek, M. T., et al. 2014, MNRAS, 442, 2560

Wuyts, E., Rigby, J. R., Sharon, K., & Gladders, M. D. 2012, ApJ, 755, 73

Yajima, H., Choi, J.-H., & Nagamine, K. 2011, MNRAS, 412, 411

Yang, H., Malhotra, S., Gronke, M., et al. 2017, ApJ, 844, 171

York, D. G., Adelman, J., Anderson, John E., J., et al. 2000, AJ, 120, 1579

Yue, B., Castellano, M., Ferrara, A., et al. 2018, ApJ, 868, 115

Zackrisson, E., Inoue, A. K., & Jensen, H. 2013, ApJ, 777, 39